


# Hall magnetohydrodynamic turbulence with a magnetic Prandtl number larger than unity

Hideaki Miura \*

*National Institute for Fusion Science, Toki, Gifu 509-5292, Japan*

Jiguan Yang and Toshiyuki Gotoh

*Department of Physical Science and Engineering, Nagoya Institute of Technology, Gokiso, Nagoya 466-8555, Japan*

 (Received 22 August 2019; revised manuscript received 19 October 2019; published 18 December 2019)

Turbulence structures with the magnetic Prandtl number larger than unity are studied by means of direct numerical simulations of homogeneous, isotropic, and incompressible Hall magnetohydrodynamic (MHD) turbulence driven by a random force. Spectral and spatial structures on the scales smaller than the ion skin depth are focused upon in this numerical paper. The numerical simulations reveal the emergence of a new power law in the velocity field whereas it is not observed in MHD turbulence simulation without the Hall term. An order estimate of the energy budget in the spectral space shows that this new power law appears in association with the Hall effect and that a balance between the Lorentz force and the viscous dissipation is crucial for formation of the power law. A resemblance to an elastic turbulence is found in the power-law-formation mechanism. Frequent eruptions of strong current ribbons accompanying strong palinstrophy density are observed, showing generation of the palinstrophy density by the Lorentz force at the scales below the ion skin depth. These properties in spectral and spatial structures characterize a high magnetic Prandtl number Hall MHD turbulence at the scales smaller than the ion skin depth.

DOI: [10.1103/PhysRevE.100.063207](https://doi.org/10.1103/PhysRevE.100.063207)

## I. INTRODUCTION

Turbulence structures are nonuniform, coherent, and even highly concentrated. A dissipative nature of magnetohydrodynamic (MHD) equations not only change smoothness of turbulent field, but also trigger change in the topology of the magnetic and/or velocity field and, thus, of the concentrated turbulence structures. The ratio of the viscosity  $\nu$  to the magnetic diffusivity  $\eta$ , or the magnetic Prandtl number  $\text{Pr}_M = \nu/\eta$ , is a crucial control parameter of MHD turbulence because of the important roles [1–3]. A clear image of high- $\text{Pr}_M$  turbulence is not established yet in comparison to turbulence in other regimes  $\text{Pr}_M \sim 1$  or  $\text{Pr}_M \ll 1$ , despite some extensive studies on this parameter regime [4–6].

Whereas the two dissipative coefficients compete to influence MHD turbulence, the Hall term, which represents a two-fluid effect in Ohm's law, can also participate in the competition between them when the ion skin depth  $d_i$  is comparable to or larger than the dissipation scales. The Hall term is known to accelerate the magnetic reconnection [3,7] and to excite dispersive waves [8,9]. The Hall term is also known to form a scaling regime of  $k^{-7/3}$  in the magnetic energy spectrum on the scale comparable to or smaller than  $d_i$  for  $\text{Pr}_M \sim 1$  [10–16], although spectral natures for  $\text{Pr}_M \gg 1$  remain unclarified. In this paper, direct numerical simulation (DNS) of homogeneous, isotropic, and incompressible Hall MHD turbulence of  $\text{Pr}_M = 10$  and 100 are carried out, focus-

ing on spectral and spatial structures on the scales smaller than  $d_i$  in order to find a clearer image of high- $\text{Pr}_M$  turbulence.

## II. DIRECT NUMERICAL SIMULATIONS

The incompressible Hall MHD equations can be expressed as

$$\partial_t u_i = -\partial_j(u_i u_j) - \partial_i p + \epsilon_{ijk} J_j B_k + \nu \partial_j \partial_j u_i + f_i, \quad (1)$$

$$\partial_t B_i = -\epsilon_{ijk} \partial_j [-\epsilon_{klm}(u_l - \epsilon_H J_l) B_m + \eta J_k], \quad (2)$$

together with the two solenoidal conditions  $\partial_i u_i = 0$  and  $\partial_i B_i = 0$ , where  $\partial_t = \partial/\partial t$  and  $\partial_j = \partial/\partial x_j$ . The symbols  $B_i$ ,  $J_i = \epsilon_{ijk} \partial_j B_k$ ,  $u_i$ , and  $f_i$  represent the  $i$ th components of the magnetic field, current density, velocity field, and random external field vectors, respectively, whereas  $\epsilon_{ijk}$  is Levi-Civita's antisymmetric tensor. The  $i$ th components of the vorticity vector  $\omega_i = \epsilon_{ijk} \partial_j u_k$  and the divorticity vector  $p_i = \epsilon_{ijk} \partial_j \omega_k = -\partial_j \partial_j u_i$  are also defined here for later use. The sum from 1 to 3 is taken for repeated suffixes. The pressure  $p$  can be obtained by Eqs. (1) and  $\partial_i u_i = 0$ . The symbol  $\epsilon_H$  is the Hall parameter (the ratio of  $d_i$  to the system size). These equations are already normalized by representative values (see Ref. [17] for normalization), and thus, we can consider  $1/\nu$  and  $1/\eta$  as the Reynolds and Lundquist numbers, respectively.

In our DNS, the vorticity equations [rotation of Eqs. (1)] and Eqs. (2) are solved numerically by the use of the pseudospectral method and the Runge-Kutta-Gill scheme under the  $(2\pi)^3$  triple-periodic boundary condition. Aliasing errors are removed by the 2/3 rule. Parameters used in this article are shown in Table I. The velocity field is driven by the

\*miura.hideaki@nifs.ac.jp

TABLE I. Parameters for DNS of Hall MHD turbulence.

Run	$N^3$	$\epsilon_H$	$\nu$	$\eta$	$\text{Pr}_M$	$R_\lambda^u$	$R_\lambda^B$
A	512 <sup>3</sup>	0.2	$1 \times 10^{-3}$	$1 \times 10^{-4}$	10	102.5	420.5
B	512 <sup>3</sup> (256 <sup>3</sup> , 1024 <sup>3</sup> )	0.2	$1 \times 10^{-2}$	$1 \times 10^{-4}$	100	11.5	77.5
C	256 <sup>3</sup>	0	$1 \times 10^{-2}$	$1 \times 10^{-4}$	100	11.4	87.5

random force  $f_i$ , which satisfies  $\partial_j f_j = 0$ . The random force is proportional to  $k^{-5/3}$  at  $k \leq 3$  and zero elsewhere in the Fourier space. The forcing range  $k \leq 3$  is chosen so that the random force perturbs the velocity field in the scale larger than the ion skin depth  $k = 1/\epsilon_H = 5$  to avoid the internal dynamics of the Hall MHD system is masked by a forcing effect.

### III. TURBULENT ENERGY SPECTRA

In Fig. 1, the kinetic energy spectrum  $E_K(k)$  and magnetic energy spectrum  $E_M(k)$  are shown for (a) runs A and B (Hall MHD) and (b) run C (MHD), respectively. The spectra have been time averaged over about 20 eddy-turn-over time at a statistically steady state. The Reynolds numbers defined by Taylor's length scale [18] ( $R_\lambda^u$  for the velocity field and  $R_\lambda^B$  for the magnetic field) in the statistically steady state are

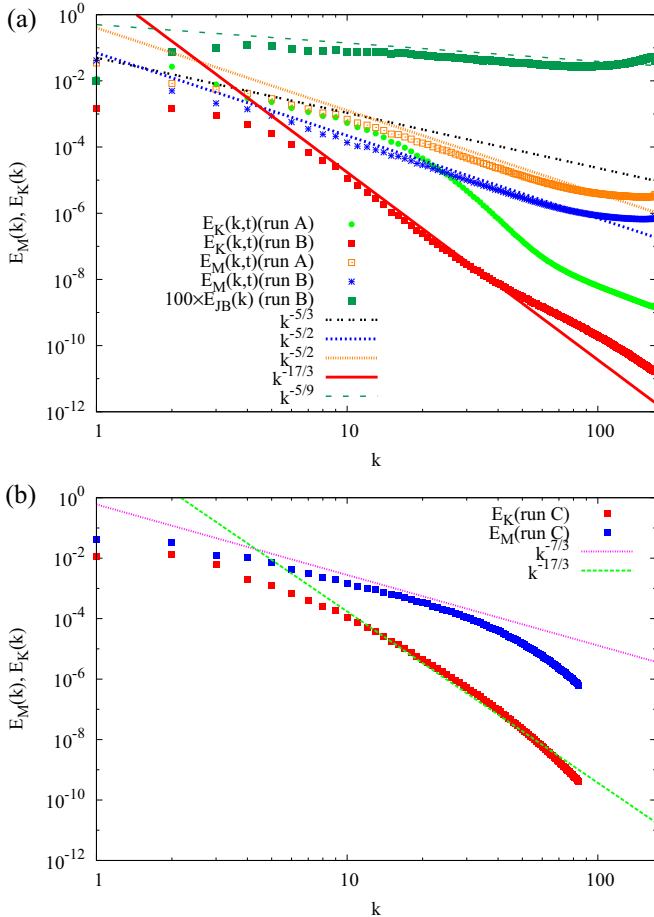


FIG. 1. Shell-averaged and time-averaged energy spectra  $E_K(k)$  and  $E_M(k)$  in (a) runs A and B and in (b) run C.

presented in Table I. The two panels (a) and (b) make a sharp contrast to each other. The two spectra  $E_K(k)$  and  $E_M(k)$  of run B in panel (a) show, at least, two power-laws  $E_M(k) \sim k^{-5/2}$  and  $E_K(k) \sim k^{-17/3}$  at  $7 \leq k \leq 35$  (hereafter, we refer to this range as mesoscale), whereas we do not see a clear power law in  $E_K(k)$  and  $E_M(k)$  in Fig. 1(b). The power-law  $E_M(k) \simeq k^{-5/2}$  is observed both in run A ( $\text{Pr}_M = 10$ ) and run B ( $\text{Pr}_M = 100$ ). The shell-averaged spectrum  $E_{JB}(k)$  of the Lorentz-force-vector  $L_i = \epsilon_{ijk} J_j B_k$  is fitted as  $k^{-5/9}$ . [Only  $E_{JB}(k)$  of run B is shown in Fig. 1(a).]

In Fig. 1(a), the magnetic energy spectra  $E_M(k)$  are influenced by the Hall term at  $k > k_H = 1/\epsilon_H = 5$ . Because of the forward magnetic energy transfer enhanced by the Hall term, the tail of  $E_M(k)$  increases slightly at  $k > 100$ . Thus, we eliminate  $k > 100$  from our discussion throughout this paper after checking the influence of the raise of the spectral tail. We verify that the power laws are insensitive to the change in the resolution by comparing the spectra in run B and that the power-law exponents are approximately  $-5/2$  for  $E_M(k)$  and  $-17/3$  for  $E_K(k)$  by the compensated energy spectra as we see below.

In Fig. 2(a),  $E_M(k)$  and  $E_K(k)$  (snapshots) of run C are compared among the computations with  $N^3 = 256^3$ ,  $512^3$ , and  $1024^3$  to examine influence of the spectral tail. The computation of  $N^3 = 1024^3$  is stopped before the spectral tail of  $E_M(k)$  rises appreciably. We can see that  $E_K(k) \propto k^{-17/3}$  on the mesoscale for all three computations. This indicates that  $E_K(k) \propto k^{-17/3}$  whether before the energy is transferred to the highest wave number ( $N^3 = 1024^3$  computation) or after the spectral tail rises ( $N^3 = 256^3$  and  $512^3$  computation) and that the power-law exponent is insensitive to the change in the resolution.

In Fig. 2(b), the compensated energy spectra  $k^{8/3} E_M(k)$ ,  $k^{5/2} E_M(k)$ , and  $k^{7/3} E_M(k)$  of run B are compared among the computations of  $N^3 = 256^3$ ,  $512^3$ , and  $1024^3$ . This figure indicates that  $k^{5/2} E_M(k)$  yields the widest range of a plateau curve for all the three resolutions, meaning that  $E_M(k) \sim k^{-5/2}$ . We also note that the spectrum  $E_M(k) \sim k^{-5/2}$  differs from  $E_M(k) \sim k^{-7/3}$  which has been expected from earlier studies [10–16]. This difference can be primarily due to a low  $R_\lambda^u$  in run B. However, recent kinetic simulations suggest  $E_M(k) \sim k^{-8/3}$  [19]. The difference among  $k^{-7/3}$ ,  $k^{-5/2}$ , and  $k^{-8/3}$  is not very large. The power-law exponent of  $E_M(k)$  associated with the Hall term may be subject to change depending on high- $\text{Pr}_M$  (low- $R_\lambda^u$ ) or kinetic effects.

A process of the energy conversion from the energy input to the final energy dissipation is discussed here. The equation of the total energy can be expressed in real space as

$$\begin{aligned}
 \partial_t (u_k u_k + B_k B_k) / 2 = & -u_i u_j \partial_j u_i - u_i \partial_i p + u_i (\epsilon_{ijk} J_j B_k) \\
 & + \nu u_i \partial_j \partial_j u_i + u_i f_i - B_i \epsilon_{ijk} \partial_j \\
 & \times [\epsilon_{kab} (u_a - \epsilon_H J_a) B_b] + \eta B_i \partial_j \partial_j B_i.
 \end{aligned} \tag{3}$$

Because of the low Reynolds number, the velocity field is damped very quickly at  $k > 3$  as we can see in Fig. 1(a), and thus, the nonlinear term  $u_i u_j \partial_j u_i$  is negligible. Under this situation, the energy from external force ( $u_i f_i$ ) at  $k \leq 3$  is first converted to the magnetic field by the

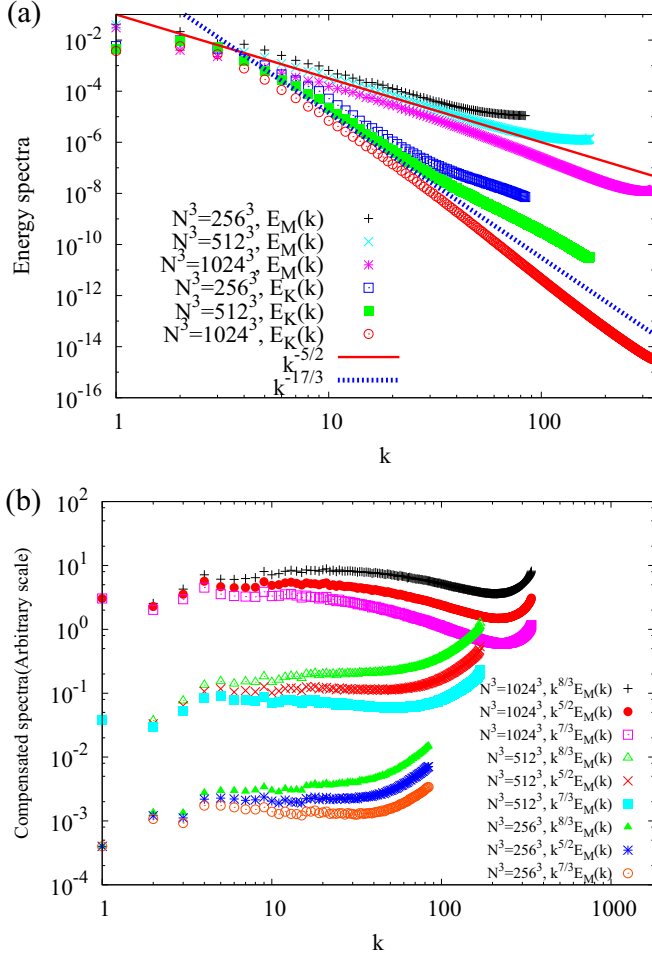


FIG. 2. (a) A comparison of  $E_M(k)$  and  $E_K(k)$  of run  $B$  among the computations of  $N^3 = 256^3$ ,  $512^3$ , and  $1024^3$ . (b) A comparison of the compensated energy spectra  $k^{8/3}E_M(k)$ ,  $k^{5/2}E_M(k)$ , and  $k^{7/3}E_M(k)$  of run  $B$  among the computations of  $N^3 = 256^3$ ,  $512^3$ , and  $1024^3$ .

dynamo term  $(-B_i \epsilon_{ijk} \partial_j [\epsilon_{kab} u_a B_b])$ . Then, the velocity field on the mesoscale can be excited only by the Lorentz force  $[u_i (\epsilon_{ijk} J_j B_k)]$ . Finally, the velocity components are attenuated by the viscous dissipation  $(\nu u_i \partial_j \partial_j u_i)$ , whereas the magnetic energy is transferred to high  $k$  by the Hall term  $\{B_i \epsilon_{ijk} \partial_j [\epsilon_{kab} (\epsilon_H J_a) B_b]\}$  [14] and dissipated by the resistive term  $(\eta B_i \partial_j \partial_j B_i)$ .

Since the spectra in Fig. 1 are shell averaged in the spectral space, we can estimate the spectra as  $E_M(k) = \sum_{[k]} |\tilde{B}_k|^2 \sim k^2 |\tilde{B}_k|^2$  and  $E_K(k) = \sum_{[k]} |\tilde{u}_k|^2 \sim k^2 |\tilde{u}_k|^2$  where the symbols  $\tilde{B}_k$  and  $\tilde{u}_k$  are Fourier coefficients of magnetic and velocity fields, respectively. The symbol  $\sum_{[k]}$  represents the shell average in the spectral space. The index  $i$  for the three-dimensional vector components for Fourier coefficients are suppressed, hereafter, for simplicity.

First, we examine the power-law  $E_M(k) \sim k^{-5/2}$  (or  $\sim k^{-7/3}$  in earlier works). We assume  $E_M(k) = \sum_{[k]} |\tilde{B}_k|^2 \sim k^\alpha$ ,  $E_K(k) = \sum_{[k]} |\tilde{u}_k|^2 \sim k^\beta$ , and  $\sum_{[k]} |\tilde{L}_k|^2 \sim k^\gamma$  on the mesoscale. Then, the Fourier coefficients  $\tilde{B}_k$ ,  $\tilde{u}_k$ , and  $\tilde{L}_k$  are estimated as  $\tilde{B}_k \sim k^{(\alpha-2)/2}$ ,  $\tilde{u}_k \sim k^{(\beta-2)/2}$ , and  $\tilde{L}_k \sim k^{(\gamma-2)/2}$ ,

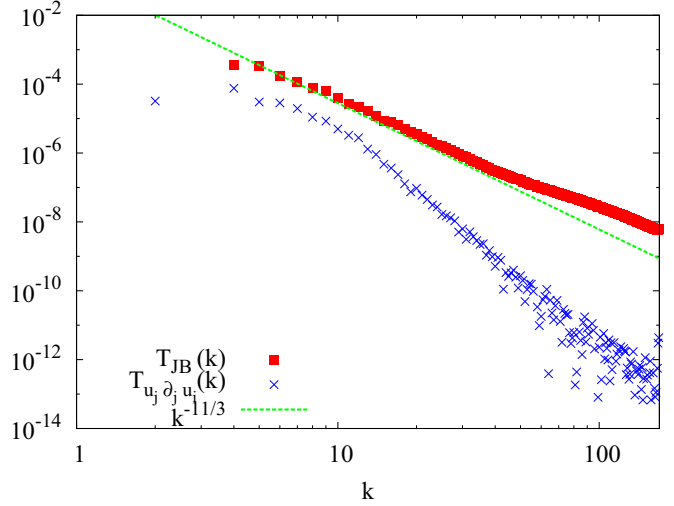


FIG. 3. Energy transfer functions  $T_{u_j \partial_j u_i}(k)$  and  $T_{JB}$  in run  $B$ . Negative values are not plotted.

respectively. The balance between the forward energy transfer by the Hall term and the resistive dissipation demands  $k \tilde{B}_k \tilde{L}_k \sim k^2 \tilde{B}_k^2$ , and the result is  $\tilde{B}_k \sim k^{\gamma/2-2}$ . By the use of  $\tilde{B}_k \sim k^{(\alpha-2)/2}$  in the original assumption and by substituting  $\alpha = -7/3$  ( $\alpha = -5/2$ ), we obtain  $\gamma = -1/3$  ( $\gamma = -1/2$ ). The combination of  $\alpha = -5/2$  and  $\gamma = -1/2$  fits to  $E_{JB}(k) = \sum_{[k]} |\tilde{L}_k|^2 \sim k^{-5/9}$  in run  $B$  better than  $\alpha = -7/3$  and  $\gamma = -1/3$ .

The power-law  $E_{JB}(k) \sim k^{-5/9}$  can be estimated in our crude ordering as follows. The Lorentz force vector, a nonlinear combination of  $B_i$  and  $J_i$ , is dominated by the contributions from  $B_i$  at a very low  $k$  and  $J_i$  on the mesoscale. Since  $B_i$  of a low  $k$  appears approximately uniform from  $J_i$  of a higher  $k$ , we can approximately replace  $B_i$  by a constant  $\tilde{B}_0$  in this analysis and estimate the Lorentz force as  $\tilde{L}_k \sim \tilde{J}_k \tilde{B}_k \sim k \tilde{B}_k B_0$ . This can be a primitive image of a whistler wave propagating along the uniform magnetic field  $B_0$  because Eq. (2) on the mesoscale or a higher  $k$  under this ordering gives  $\omega \sim \epsilon_H B_0 k^2$  ( $\omega$  is the frequency), a dispersion relation similar to that of the whistler wave [8]. In this ordering,  $\tilde{L}_k \sim k \tilde{B}_k \sim k^{\alpha/2}$  whereas we have assumed  $\tilde{L}_k \sim k^{(\gamma-2)/2}$  initially. By the use of  $\alpha = -5/2$  and  $\gamma = -5/9$ , the two orderings result in  $\tilde{L}_k \sim k^{\alpha/2} \sim k^{-5/4}$  and  $\tilde{L}_k \sim k^{(\gamma-2)/2} \sim k^{-23/18}$ , respectively. The orderings agree with each other approximately.

Next, the energy balance between the energy transfer in the velocity field is examined. For this purpose, the energy transfer functions  $T_{u_j \partial_j u_i}(k)$  and  $T_{JB}(k)$  in run  $B$  are shown in Fig. 3. These two functions are the shell-averaged representations of  $u_i (u_j \partial_j) u_i$  and  $u_i (\epsilon_{ijk} J_j B_k)$  in the Fourier space, respectively. The former is negligible to the latter on the mesoscale and  $T_{JB}(k) \sim k^{-11/3}$  in Fig. 3. By considering the balance between  $T_{JB}(k) \sim k^{-11/3}$  and the viscous dissipation  $\sum_{[k]} \nu u_i \partial_j \partial_j u_i \sim k^2 k^2 k^{\beta-2}$ , we obtain  $k^{-11/3} \sim k^{\beta+2}$  and, thus,  $\beta = -17/3$ , a good agreement with the numerical result in Fig. 1(a).

The analysis in the above paragraph depends on the observation of  $T_{J \times B}(k) \sim k^{-11/3}$ . From the definition  $T_{JB}(k) \sim k^2 \tilde{u}_k \tilde{L}_k \sim k^2 k^{(\beta-2)/2} k^{(\gamma-2)/2} \sim k^{(\beta+\gamma)/2}$ . However, the Lorentz force should be dominated by the combination of  $J_i$  on the mesoscale and the magnetic field of low

$k$ ,  $\tilde{L}_k \sim \tilde{J}_k B_0$ , and thus,  $T_{JB}(k) \sim k^2 k^{(\alpha-2)/2} k^{1+(\beta-2)/2} B_0$ . By substituting  $\alpha = -5/2$  and  $\beta = -17/3$ ,  $T_{JB}(k) \sim k^{-37/12}$ . We consider that the difference of the exponent  $-11/3$  to  $-49/12$  is acceptable within this crude estimation.

As we have shown in the above, our ordering gives a consistent explanation from the power-law  $E_M(k) \sim k^{-5/2}$  to  $E_K(k) \sim k^{-17/3}$  via collateral power-laws  $\sum_{|k|} |\tilde{L}_k|^2 \sim k^{-5/9}$  and  $T_{JB}(k) \sim k^{-11/3}$ . In other words, the power-law  $E_K(k) \sim k^{-17/3}$  on the mesoscale can appear in association with the power law of  $E_M(k) \sim k^{-5/2}$ . Thus, we assert that the spectral structure of  $E_K(k)$  is determined by the spectral structure of the magnetic field on the mesoscale.

At the end of the spectral analysis, we comment on a few points in our simulations. The forcing range of  $k \leq 3$  is set not to overlap the subion scale at  $k > k_H = 1/\epsilon_H = 5$ . This is necessary to avoid interference between the force and the subion scales. We need simulations with a larger  $N$  for separating the forcing range from the ion skin depth scale sufficiently. Such larger simulations should be performed in the near future.

We still keep in mind an intrinsic difficulty in determining the power-law exponent. A recent article on hydrodynamic turbulence reports that the power-law exponent of the energy spectrum should be corrected by their huge  $N^3 = 12\,288^3$  computations [20]. In the case of our paper, we need a wider range of the mesoscale which should be enabled by a larger magnetic Prandtl number. For such a simulation, we need an extremely huge number of grid points.

The third comment is on a similarity between the scaling law in the above and that reported on elastic turbulence simulations [21]. In the elastic turbulence simulations, the fluid inertia  $-u_j \partial_j u_i$  is so weak that the Navier-Stokes equations are approximately linear and the energy spectrum should decay exponentially. Nevertheless, a power law in the velocity field is observed because an interaction with polymers excite the velocity on the dissipation scale. This scenario is very similar to our numerical results in the sense that the power-law  $E_M(k) \sim k^{-17/3}$  is formed by the interaction with the magnetic field (Lorentz force) at the dissipation scale.

#### IV. TURBULENT STRUCTURES

Although Hall MHD simulations show a power law in the spectral space which does not appear in (non-Hall) MHD turbulence, differences of Hall MHD turbulence from that of MHD turbulence are found in the real space too. Isosurfaces of the enstrophy density  $Q = \omega_i \omega_i / 2$  (green or gray in the printed version), palinstrophy density  $P = p_i p_i / 2$  (red or dark gray in the printed version) (recall  $p_i = \epsilon_{ijk} \partial_j \omega_k$ ), and current density  $I = J_i J_i / 2$  (light gray) in runs A–C are drawn in Figs. 4(a)–4(c), respectively, their *in situ* visualization software VISMO [22]. Isosurfaces of  $P$  are omitted from (a) for clarity in the figure. The thresholds of the isosurfaces are three times the standard deviation above the mean value of the quantities. In Figs. 4(a) and 4(b), a ribbonlike structure of  $I$  is formed. The isosurfaces are often elongated over a long

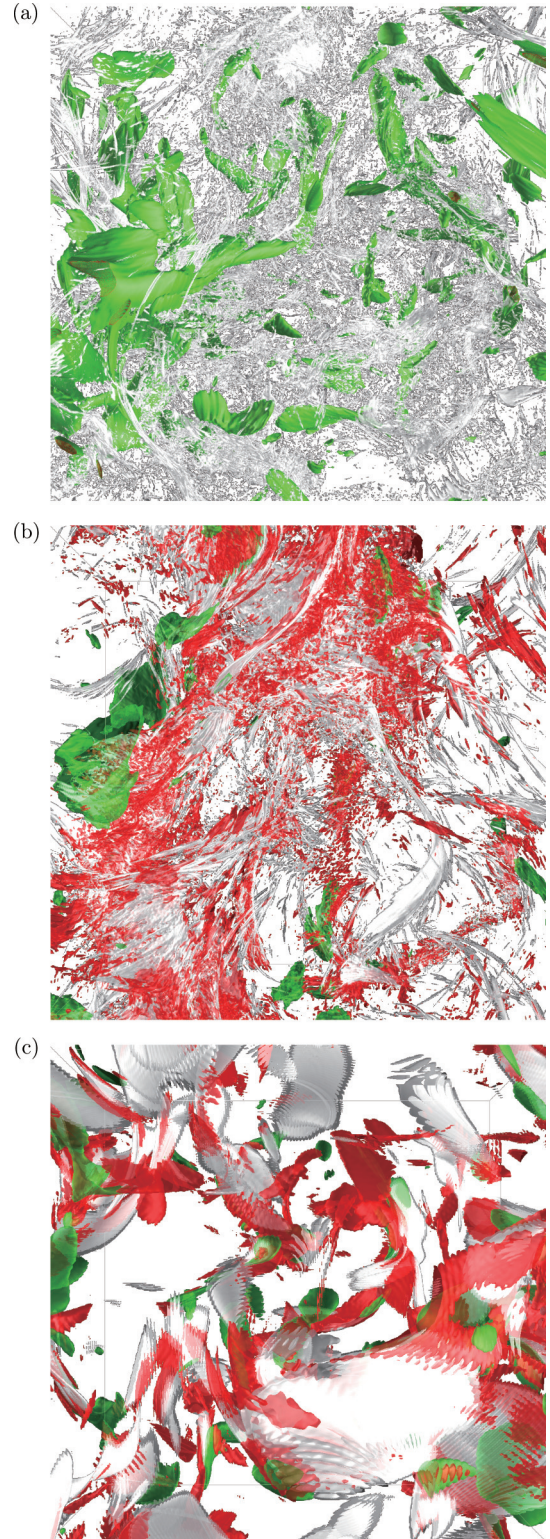


FIG. 4. Isosurfaces of the enstrophy density  $Q$  (green, or gray in the printed version), the palinstrophy  $P$  (red, or dark gray in the printed version), and current density  $I$  (light gray) in runs A–C in (a)–(c), respectively. Isosurfaces of the palinstrophy density  $P$  (red) are drawn in (b) and (c), whereas they are not drawn in (a) for clarity in the figure.

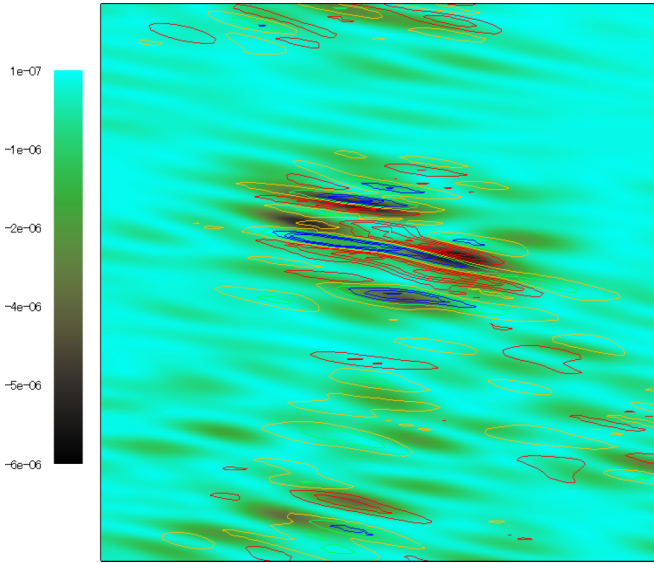


FIG. 5. Contours of the viscous term  $-v u_i \partial_k \partial_k u_i$  (color map) and Lorentz-force term  $u_i (\epsilon_{ijk} J_j B_k)$  (contour lines) in Eq. (3) of run *B* on a plane of  $128 \times 128$  grid points.

distance especially in Fig. 4(b), and the appearance of the isosurfaces is different from that of Hall MHD turbulence of  $\text{Pr}_M = 1$  reported in Ref. [14]. The isosurfaces of  $Q$  and  $I$  are fully separated from each other, whereas  $P$  and  $I$  overlap each other. An inspection of the time series of the isosurfaces can show that the current ribbons erupt frequently and propagate quickly along the magnetic field, although we omit the time-sequence figures. This dynamic phenomenon is not observed in run *C*. In Fig. 4(c), isosurfaces of  $Q$  and  $I$  of run *C* are sheetlike as are often observed in MHD turbulence (see Biskamp [1], for example), and a ribbonlike structure as in Figs. 4(a) and 4(b) is not observed in (c).

Here, we comment on vortex structures in Figs. 4(a) and 4(b). The green isosurfaces for  $Q$  in Fig. 4(a) are often tubular, suggesting that they are formed by a rollup of a vortex sheet and that high- $k$  components of the velocity field are generated by hydrodynamic motions autonomously. On the contrary, the green isosurfaces in Fig. 4(b) do not indicate specific structures, whereas the red isosurfaces for  $P$  are observed together with the gray isosurfaces for  $I$ . Since the Lorentz force is strong where  $I$  is large, Fig. 4(b) indicates that the velocity components at high  $k$  (including the mesoscale we mentioned in the spectral analysis) are generated by the Lorentz force, being consistent with the ordering analysis in *turbulent energy spectra*. In other words, the velocity components at high  $k$  are generated primarily by the magnetic field.

In Fig. 5, contours of the viscous term  $-v u_i \partial_k \partial_k u_i = v u_k p_k$  (color map) and the Lorentz-force term  $u_i (\epsilon_{ijk} J_j B_k)$  (contour lines) in Eq. (3) of run *B* are drawn on a plane of 128 grid points each in the two directions. Dark-color regions where the viscous term has a large negative value are placed close to red or blue contours where the Lorentz has a large positive or negative value. We have verified that contours of not only the viscous and Lorentz-force terms, but also dynamo and Hall terms stay in the neighborhood with each other.

This observation can be understood as follows. The viscous term  $v u_k p_k$  becomes large where the Lorentz term generates high- $k$  velocity components. In fact, isosurfaces of  $P$  accompanied by those of  $I$  in Fig. 4(b) disappear if  $p_i$  is filtered by the low-pass filter of which cutoff wave number is at the middle of the scaling laws in Fig. 1 or at lower wave numbers. The Hall term (the rotation of the Lorentz force) is also large there. The dynamo term can be also large there because this term is coupled with the Lorentz force strongly for energy exchange between the velocity and the magnetic field. These observations support the ordering analysis in the spectral space from a point of view of real-space analysis.

## V. CONCLUDING REMARKS

DNSs of Hall MHD turbulence have been carried for clarifying basic fluid-dynamic aspects of high- $\text{Pr}_M$  MHD turbulence on the scale smaller than the ion skin depth  $d_i$ . The numerical results show that the power-law  $E_K(k) \sim k^{-17/3}$  can be formed in association with the scaling law of  $E_M(k) \sim k^{-5/2}$  as a consequence of the balance between the Lorentz force and the dissipation term. Our result shows that a power law can appear in  $E_K(k)$  on the scale smaller than  $d_i$  for turbulence with  $\text{Pr}_M \gg 1$ , although special attention has been paid to a power law in  $E_M(k)$ .

In the real space, current ribbons prevail in a turbulent field, propagating rapidly and accompanying the palinstrophy density which is generated by the Lorentz force. The real-space observation supports the analysis on the power law in the spectral space. The observation of a rapidly propagating current ribbon is also consistent with a finite role of the whistler wave, which has been mentioned in the power-law analysis. Since the power-law range observed in this paper is not sufficiently wide, we need simulations of a larger magnetic Prandtl number with a larger number of grid points to enable a separation between the scales of the external force and subion skin depth. A larger magnetic Prandtl number widens the mesoscale range we discussed in this article. Finally, we note that there is a possibility that the interpretation of the power law in this article could be affected by an insufficient dissipation or a numerical resolution. Simulations using a hyperdiffusivity and/or larger number of grid points are effective for further study and now in progress.

Our subject shares an outline of mechanism to generate a power law in the velocity field with an elastic turbulence. We consider that this subject can be studied not only as a subject of plasma physics, but also in a wider context of turbulence phenomena.

## ACKNOWLEDGMENTS

This research was supported partially by JSPS KAKENHI Grants No. JP17K05734 and No. JP15H02218, Japan. The numerical simulations were performed on the FUJITSU FX100 supercomputer *Plasma Simulator* of NIFS with the support and under the auspices of the NIFS Collaboration Research Program (Grants No. NIFS15KNSS053 and No. NIFS15KNSS038) and on the FUJITSU Oakforest-PACS supercomputer of the University of Tokyo, being partially

supported by the *Joint Usage/Research Center for Interdisciplinary Large-Scale Information Infrastructures* in Japan. Development of some numerical codes used in this paper was

supported, in part, by the Code Development Support Program of the Numerical Simulation Reactor Research Project (NSRP), NIFS.

- 
- [1] D. Biskamp, *Magnetohydrodynamic Turbulence* (Cambridge University Press, Cambridge, 2003).
  - [2] P. A. Davidson, *Turbulence in Rotating, Stratified and Electrically Conducting Fluids* (Cambridge University Press, Cambridge, 2013).
  - [3] D. Smith, S. Ghosh, P. Dmitruk, and W. H. Matthaeus, *Geophys. Res. Lett.* **31**, L02805 (2004).
  - [4] A. Brandenburg, *Astrophys. J.* **791**, 12 (2014).
  - [5] A. A. Schekochihin, S. C. Cowley, and S. F. Taylor, *Astrophys. J.* **612**, 276 (2004).
  - [6] T. A. Yousef, F. Rincon, and A. A. Schekochihin, *J. Fluid Mech.* **575**, 111 (2007).
  - [7] S. Donato, A. Greco, W. H. Matthaeus, S. Servidio, and P. Dmitruk, *J. Geophys. Res.: Space Phys.* **118**, 4033 (2013).
  - [8] S. Ohsaki and S. Mahajan, *Phys. Plasmas* **11**, 898 (2004).
  - [9] S. M. Mahajan and H. Miura, *J. Plasma Phys.* **75**, 145 (2009).
  - [10] S. Galtier and E. Buchlin, *Astrophys. J.* **656**, 560 (2007).
  - [11] P. Mininni, A. Alexakis, and A. Pouquet, *J. Plasma Phys.* **73**, 377 (2007).
  - [12] S. Galtier, *Phys. Rev. E* **77**, 015302(R) (2008).
  - [13] D. Hori and H. Miura, *Plasma Fusion Res.* **3**, S1053 (2008).
  - [14] H. Miura and K. Araki, *Phys. Plasmas* **21**, 072313 (2014).
  - [15] J. E. Stawarz and A. Pouquet, *Phys. Rev. E* **92**, 063102 (2015).
  - [16] H. Miura, K. Araki, and F. Hamba, *J. Comput. Phys.* **316**, 385 (2016).
  - [17] H. Miura, *Fluids* **4**, 46 (2019).
  - [18] U. Frisch, *Turbulence: The Legacy of A. N. Kolmogorov* (Cambridge University Press, Cambridge, 1995).
  - [19] C. A. González, T. N. Parashar, D. Gomez, W. H. Matthaeus, and P. Dmitruk, *Phys. Plasmas* **26**, 012306 (2019).
  - [20] T. Ishihara, K. Morishita, M. Yokokawa, A. Uno, and Y. Kaneda, *Phys. Rev. Fluids* **1**, 082403(R) (2016).
  - [21] T. Watanabe and T. Gotoh, *J. Fluid Mech.* **717**, 535 (2013).
  - [22] N. Ohno and H. Ohtani, *Plasma Fus. Res.* **9**, 3401071 (2014).